Topology Optimization of Thermal Cloaks in Euclidean Spaces and Manifolds using an Extended Level Set Method

Xiaoqiang Xu[a], Xianfeng David Gu[b,c], Shikui Chen[a,*]

[a] *Department of Mechanical Engineering, State University of New York at Stony Brook, Stony Brook, 11794, NY, USA*
[b] *Department of Computer Science, State University of New York at Stony Brook, Stony Brook, 11794, NY, USA*
[c] *Department of Applied Mathematics and Statistics, State University of New York at Stony Brook, Stony Brook, 11794, NY, USA*

Abstract

Thermal cloaks are devices designed to shield an object against thermal detection, which have attracted growing interest in research. This paper proposes to design thermal cloaks using the level-set-based shape and topology optimization in the context of pure heat conduction. The cloaking effect is achieved by optimizing the distribution of two bulk heat conductive materials to eliminate the temperature disturbance induced by the introduction of the insulator (cloaking region) into a homogeneous thermal conduction medium. The optimized thermal cloaks are free of high anisotropy and nonhomogeneity commonly seen in the popular transformation thermotics or scattering cancellation methods. Due to the clear boundary characteristic of the level set representation, no sophisticated filtering techniques are required to suppress the appearance of "gray regions" as opposed to the density-based topology optimization methods. Considering the fact that the device components that need to be thermally cloaked, e.g., sensors, can take an arbitrary free-form shape, a conformal thermal cloak on manifold is also topologically optimized using the extended level set method (X-LSM), which has not been reported in the literature. The structural boundary is evolved by solving the (modified) Hamilton-Jacobi equation. The feasibility and robustness of the proposed method to design thermal meta-devices with cloaking functionality are demonstrated through a number of 2D and 3D (solid and shell) numerical examples with different cloaking regions (circular, human-shaped, spherical and curved circular). This work may shed light on further exploration of the thermal meta-devices in the heat flux manipulation regime.

Keywords: Thermal cloak, Heat flux manipulation, Topology Optimization, Level set method, Extended Level Set Method

1. Introduction

How to conceal an object has fascinated people for a long time. The invisibility cloak in *Harry Potter* is too magic to be perfectly realized, owing to the wave nature of light [1]. However, thanks to the two pioneering works [2, 3], some lights were shed on guiding light around an object as if nothing was there. This original concept of cloaking from the optical field has since then been expanded into various fields, e.g., thermal cloaks [4–6], acoustic cloaks [7] and magnetic cloaks [8], to name a few. Inspired by the way the light traveling path is altered to render optical invisibility in the wave system, researchers have attempted

*Corresponding author
Email address: Shikui.Chen@stonybrook.edu (Shikui Chen)

to manipulate the heat flow in a desired manner using meticulously designed metamaterials to achieve a variety of thermal functionalities in the diffusion system [9–13], such as thermal cloaks [4, 5, 14], thermal concentrators [15, 16], thermal rotators [17–19] and thermal camouflages [20, 21].

Two popular methods for designing such thermal metamaterials are the scattering cancellation method [22, 23] and the transformation thermotics method [6, 12], inspired and developed by the pioneering transformation optics [2, 3]. The basic idea behind transformation thermotics is that to maintain the invariance of the domain equation under coordinate transformation, the related physics property, i.e., thermal conductivity tensor, must be properly modified. As a result, the thermal metamaterials obtained through transformation thermotics often exhibit high anisotropy and inhomogeneity, posing a significant challenge to physical realization. A common treatment is to employ a multi-layered structure [19, 24], but often at the expense of a certain loss of accuracy. We briefly mention some of the preceding research endeavors using the aforementioned methods. Imran et al. [24] and Dede et al. [25] explored the heat flux control devices taking into account the convection effect. Vemuri et al. [26] managed to guide the conductive heat flux by properly positioning and orienting the nominally isotropic material. Moccia et al. [27] realized the independent manipulation of heat and electrical current, pushing one step further toward the "transformation multiphysics". An intelligent thermal metamaterial was developed in [16], which exhibits either cloaking or concentrating functionality depending on the ambient temperature. An intriguing macroscopic thermal diode was subsequently created and experimentally validated in [28].

Attempts have also been made to design thermal metamaterials using natural materials to avoid high anisotropy. For example, a thermal camouflage device was demonstrated in [21], which was directly derived from the conduction equation and could produce a different thermal scattering signature than expected. The research studies in [4, 5, 29, 30] focused on the experimental validation of thermal meta-devices with various functionalities.

As an alternative, numerical optimization has been employed to design thermal metamaterials. Dede et al. [31] examined the thermal-composite design for heat flux shielding, focusing, and reversal by optimizing the inclusion angles in a surrounding medium. Peralta et al. [32] devised a thermal concentrator using a continuous optimization approach by considering a metadevice with a quantitatively characterizable microstructure consisting of a laminate of two materials with contrasting thermal conductivities. The optimization was conducted considering both the orientation and relative thickness of materials as the design variables. Subsequent work from Peralta et al. [33] ensured the fabricability of the devices using a Discrete Material Optimization (DMO) technique. The versatility and potential of the continuous optimization approach have also been demonstrated in the design of metadevices for heat flux manipulation in transient regimes [34], not limited to only steady conduction problems. By using two macroscopically distinguishable bulk materials, several metadevices were devised using the density-based topology optimization method with different application purposes, e.g., thermal [35], mechanical [36] and later thermo-mechanical problems [37]. The thermo-mechanical metadevices from [37] also explored square cloaking regions besides conventional circular or annular geometries. Seo et al. [38] proposed a multi-scale topology optimization method using only a single variable for heat flux control purposes. The multi-scale method was shown to be more advantageous over the various composition ratios of the highly conductive material than the single-scale counterpart. Yet, the optimized designs did not have quite crisp boundaries. Sha et al. [39] came up with an illusion device using density-

based topology optimization, where the heat source is camouflaged while keeping the exterior temperature field unaltered. Recent work from Sha et al. [17] combined the transformation thermotics and topology optimization to successfully design thermal meta-devices with omnidirectional thermal functionalities. To suppress the appearance of "gray region", i.e., intermediate densities, sophisticated filtering techniques [40] are often required in the density-based optimization methods for thermal metadevices design [35–37]. A number of papers [14, 15, 41] dealt with the topology optimization of thermal meta-devices with a level set representation using the covariance matrix adaptation evolution strategy (CMA-ES) to search for the optimal designs. However, most existing designs only focus on 2D planar cases with canonical cloaking regions, i.e., circular shapes. Moreover, the 3D solid thermal cloak obtained using numerical optimization has yet to be reported. Since the device components that need to be thermally cloaked, e.g., sensors, can take an arbitrary free-form shape, a conformal thermal cloak on the manifold is strongly desired, which has not been investigated in the literature.

In this study, we try to contribute by designing thermal cloaks by means of level set based topology optimization. The objective function will be the least square error in the current design temperature field from a predefined reference temperature field in a specific evaluation domain. Two bulk materials with separate thermal conductivity will be properly distributed in the design domain to minimize the temperature disturbance in the evaluation domain. The clear boundaries between different material phases facilitate the generation of 3D models and the carrying out of physical experiments. No extra filtering techniques are needed in the optimization process. A conformal manifold thermal cloak is also topologically optimized using the extended level set method [42] by incorporating conformal geometry theory [43], where the hurdles of dynamic boundary evolution on free-form surfaces are overcome by solving a modified Hamilton-Jacobi equation on the 2D parameter domain (See Section 2.3 for details). The optimized multimaterial configuration exhibits the thermal cloaking functionality, and does not exhibit material anisotropy and inhomogeneity. The effectiveness and robustness of the proposed method are demonstrated through a number of 2D and 3D (solid and shell) numerical examples with different cloaking regions (circular, human-shaped, spherical and curved circular).

This paper is organized as follows: Section 2 will provide the problem formulation and shape sensitivity analysis. Numerical examples, including 2D and 3D designs, will be presented in Section 3. Section 4 will contain some discussions with closing remarks.

2. Shape and topology optimization of thermal cloaks

2.1. Problem formulation

This paper is focused on designing thermal cloaks using level-set-based topology optimization. For simplicity, we first consider a 2D steady-state heat conduction problem. It is assumed that all associated physical properties are isotropic. The governing equations for pure heat conduction phenomena are given as follows:

$$\begin{aligned} -k\nabla^2 T &= 0, \ in \ \ \Omega \\ k\nabla T \cdot \mathbf{n} &= 0, \ on \ \ \Gamma_H \\ T &= T_h, \ \ on \ \ \Gamma_{D1} \\ T &= T_l, \ \ on \ \ \Gamma_{D2} \end{aligned} \tag{1}$$

where k is the thermal conductivity, T is the state variable temperature, $\mathbf{n}$ is the outward unit vector of the structural boundary. There is no body heat source term, nor boundary heat flux. As shown in Figure 1, the whole computational model consists of the insulator domain Ω_{ins}, the design domain Ω_D and the outer domain Ω_{out}. Two Dirichlet boundary conditions are applied with $T_h = 333.15K$ and

$T_l = 273.15K$ on the left and right edges in red and black color, respectively. All other boundaries are adiabatic. Ω_{ins} is the region of interest that we want to cloak. By cloaking, it means that there should be no temperature gradient within Ω_{ins}. Suppose we simply dig the insulator domain Ω_{ins} out of a reference domain, which is solely filled with single material iron. In that case, it will disturb the temperature distribution on Ω_{out}. Assuming a thermal sensor is employed to evaluate the temperature perturbation in Ω_{out}, it would detect the existence of the insulator region, i.e., it is not clocked. This makes it reasonable to introduce some copper with a higher thermal conductivity to offset for the extremely low thermal conductivity brought by the insulator region Ω_{in}. An optimal distribution between iron and copper in the design domain Ω_D can be sought after using topology optimization. Ω_{out} will always be filled with iron.

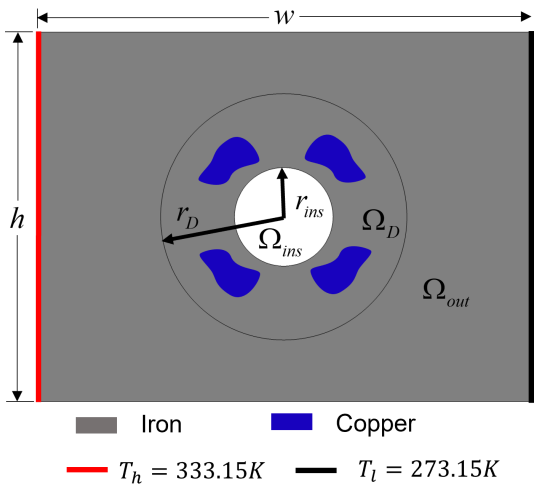

Figure 1: The diagram of a thermal cloak with a circular insulator. $w = 4, h = 3, r_{ins} = 0.4, r_D = 1$. The thermal conductivities for copper and iron are set to be $k_{copper} = 400W/(m \cdot K), k_{iron} = 67W/(m \cdot K)$.

The objective of the optimization is to minimize the least square error between the temperature fields in the external evaluation domain Ω_{out}. The formal optimization problem is formulated as follows:

$$\begin{aligned} \underset{\Phi}{Inf} \quad & J = \frac{1}{J_n}\int_{\Omega_{out}} |T - T_{ref}|^2 d\Omega, \\ s.t. \quad & a(T, \bar{T}) = 0, \ \forall \bar{T} \in U_{ad}, \end{aligned} \tag{2}$$

where $a(T, \bar{T}) = \int_\Omega k\nabla T \cdot \nabla \bar{T} d\Omega$. $\bar{T}$ is the test function and U_{ad} is the space of the virtual temperature field satisfying the same boundary conditions. The reference temperature field T_{ref} with uniform gradient is generated by filling all the computational domain with iron. J_n is a constant normalization term to keep the objective value in a moderate range. J_n is given as:

$$J_n = \int_{\Omega_{out}} |T_0 - T_{ref}|^2 d\Omega, \tag{3}$$

where T_0 is the temperature field when the design domain Ω_D is filled with only iron in the presence of central insulator. The Φ refers to the level set function, which functions as the design variable and embed the structural boundaries in its zero contours.

Pioneered by Sethian and Wiegmann [44] and further completed by Allaire [45] and Wang [46], respectively, the level set method has become a promising shape and topology optimization approach. A clear boundary between different phases can be generated and maintained during the optimization process, which is a much desired property when a detailed description of the boundary is required. The structural boundary is implicitly represented as the zero contour of a one-higher dimensional level set function. The level set function is defined on a fixed background grid in the conventional level set framework. The structural design is implicitly embedded in the level set function $\Phi(\mathbf{x}, t)$ as follows:

$$\begin{cases} \Phi(\mathbf{x}, t) > 0, & x \in \Omega, & \text{material} \\ \Phi(\mathbf{x}, t) = 0, & x \in \partial\Omega, & \text{boundary} \\ \Phi(\mathbf{x}, t) < 0, & x \in D/\Omega, & \text{void} \end{cases} \tag{4}$$

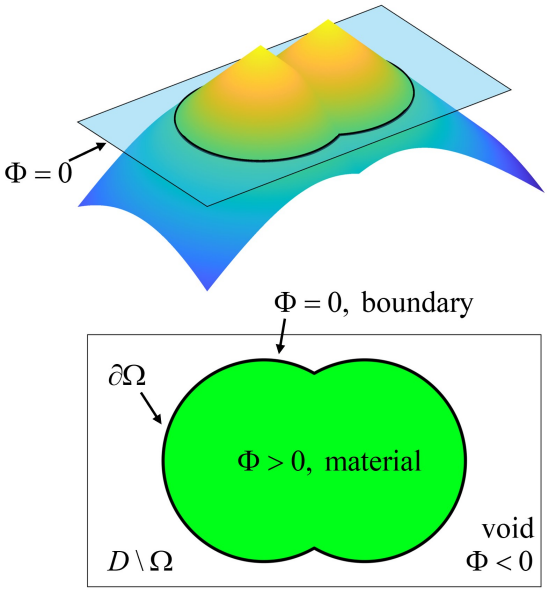

Figure 2: The level set representation of a 2D design

The level set representation of a 2D design is shown in Figure 2. For the structural boundary, it always satisfies the equation $\Phi(\mathbf{x}, t) = 0$. By differentiating both sides of the equation with respect to a pseudo time t, we could obtain the Hamilton-Jacobi (H-J) equation [47]:

$$\frac{\partial \Phi(\mathbf{x}, t)}{\partial t} - V_n \cdot |\nabla \Phi| = 0, \tag{5}$$

where $V_n = V \cdot (-\frac{\nabla \Phi}{|\nabla \Phi|}) = \frac{d\mathbf{x}}{dt} \cdot (-\frac{\nabla \Phi}{|\nabla \Phi|})$. The update of the level set function is realized by solving the above H-J equation iteratively to evolve the structural boundary. The normal velocity V_n can be obtained from shape sensitivity analysis, which is usually derived using the adjoint method.

In this study, the level set function Φ is defined on the design domain Ω_D. Specifically, $\Phi > 0$ refers to the copper domain Ω_{copper} and $\Phi < 0$ represents the iron domain Ω_{iron}. The structural boundary between copper and iron is given as $\Phi = 0$. There is no void phase in the design domain Ω_D.

2.2. Shape sensitivity analysis

As can be seen from equation (5), the normal velocity V_n is needed to solve the H-J equation. V_n can be obtained from shape sensitivity analysis [45, 46]. In this study, we employ the material derivative method [48] and adjoint method [49] to derive the shape derivative.

The Lagrangian of the optimization problem is defined as

$$L = J(T) + a(T, \bar{T}). \tag{6}$$

The material derivative of the Lagrangian is given:

$$\frac{DL}{Dt} = \frac{DJ(T)}{Dt} + \frac{Da(T, \bar{T})}{Dt}. \tag{7}$$

In this problem formulation, the objective function is evaluated on Ω_{out}, which is different from the design domain Ω_D. We rewrite the objective function J as follows:

$$\begin{aligned} J &= \frac{1}{J_n} \int_{\Omega_{out}} |T - T_{ref}|^2 d\Omega \\ &= \frac{1}{J_n} \int_{\Omega} g(x) \cdot |T - T_{ref}|^2 d\Omega, \end{aligned} \tag{8}$$

where $g(x)$ is a window function, which takes value 1 in domain Ω_{out}, and 0 in domain Ω_D and Ω_{ins}.

The material derivative of the objective function $J(T)$ is:

$$\begin{aligned} \frac{DJ(T)}{Dt} &= \frac{1}{J_n} \int_{\Omega} 2g(x) \cdot (T - T_{ref}) \cdot T' d\Omega \\ &+ \frac{1}{J_n} \int_{\partial\Omega} g(x) \cdot |T - T_{ref}|^2 \cdot V_n ds. \end{aligned} \tag{9}$$

The material derivative of the weak-form governing equation is:

$$\frac{Da(T,\bar{T})}{Dt} = \int_\Omega k[\nabla T' \cdot \nabla \bar{T} + \nabla T \cdot \nabla \bar{T}']d\Omega + \int_{\partial\Omega} k\nabla T \cdot \nabla \bar{T} \cdot V_n ds. \tag{10}$$

Collecting all the terms containing $\bar{T}'$ as follows:

$$\int_\Omega k\nabla T \cdot \nabla \bar{T}' d\Omega = 0. \tag{11}$$

we recover the weak form of the state equation as $a(T, \bar{T}') = 0$, for $\forall \bar{T}' \in U_{ad}$. Collecting the terms containing T' and making the sum equal to zero, we can obtain the adjoint equation:

$$\frac{1}{J_n}\int_\Omega 2g(x) \cdot (T - T_{ref}) \cdot T' d\Omega + \int_\Omega k\nabla T' \cdot \nabla \bar{T} d\Omega = 0. \tag{12}$$

The above adjoint equation (12) is solved for $\bar{T}$. The remaining part for the material derivatives of the Lagrangian L reads:

$$\frac{DL}{Dt} = \frac{1}{J_n}\int_{\partial\Omega} g(x) \cdot |T - T_{ref}|^2 \cdot V_n ds + \int_{\partial\Omega} k\nabla T \cdot \nabla \bar{T} \cdot V_n ds \tag{13}$$

Applying the steepest descent method, the design velocity field can be constructed as:

$$V_n = -\frac{1}{J_n} g(x) \cdot |T - T_{ref}|^2 - k\nabla T \cdot \nabla \bar{T}. \tag{14}$$

2.3. Conformal mapping theory and extended level set method (X-LSM)

The conventional level set formulations detailed in subsections 2.1 and 2.2 are well suited for shape and topology optimization problems in Euclidean space (2D planar and 3D solid cases). However, they are not quite convenient for shape and topology optimization on Riemannian manifolds since the level set function Φ is typically defined on fixed Euclidean grids. By incorporating the conformal geometry theory [43], the extended level set method (X-LSM) [42] elegantly extends the level set framework from Euclidean space to Riemannian space, enabling us to do shape and topology optimization on free-form surfaces in a fast and robust manner. A conformal mapping is essentially a function that locally preserves angles, but not necessarily lengths. A vivid representation of this angle preservation characteristic is shown in Figure 3, where the infinitesimal circles are mapped to infinitesimal circles from the 3D human face to a 2D disk.

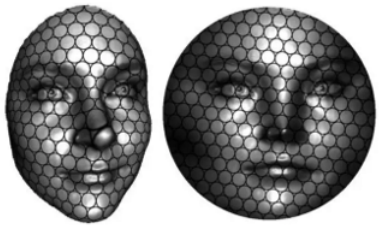

Figure 3: Conformal mapping from 3D surface to 2D disk [43]

Based on the fact that the covariant derivatives on the manifold can be represented by the Euclidean gradient operators multiplied by a scalar with the conformal parameterization, in X-LSM, the original Hamilton-Jacobi equation defined on manifolds can now be equivalently solved on the 2D parameter domain with a modified form:

$$\frac{\partial \Phi(\mathbf{x}, t)}{\partial t} - e^{-\lambda} V_n \cdot |\nabla \Phi| = 0, \tag{15}$$

where $e^{2\lambda}$ is the conformal factor associated with this conformal parameterization. The surface-to-plane conformal parameterization is computed based on Hamilton's Ricci flow theory [50, 51]. By solving this modified Hamilton-Jacobi equation (15) on the 2D parameter domain, the structural boundary evolution is now performed on 2D plane utilizing the well established finite difference scheme. The X-LSM not only maintains the benefits of the conventional level set method, e.g., clear boundary description and flexibility in handling topological changes, but also overcomes the hurdles of dynamic boundary evolution on free-form surfaces. The computational cost and algorithm complexity will also be considerably reduced. Based on X-LSM, a number of topology optimization problems on manifolds were resolved, such as soft robot design problems [52, 53] and thermal problems [54]. A recently proposed dimension reduction level set method (DR-LSM) by Xu et al. [55] takes one step further by transferring both the physics governing equation and the Hamilton-Jacobi equation from manifold in 3D space to the 2D parameter domain. The equivalence of this dimension reduction formulation and the induced computational cost saving capability are systematically investigated. For interested readers, please refer to [42, 55] for detailed mathematical derivations. In this study, the extended level set method (X-LSM) will be employed to design a thermal cloak on a free-form surface. The flowchart for the X-LSM is depicted in Figure 4.

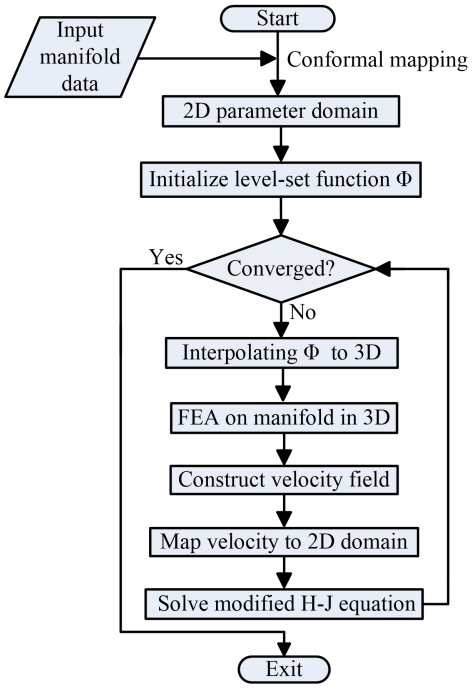

Figure 4: The flowchart of the X-LSM

3. Numerical examples

In this section, in total four numerical examples are covered to demonstrate the validity and feasibility of the proposed methodology in designing thermal cloaks, including 2D cloaks with circular/human-shaped insulators, 3D solid cloak with a spherical insulator and a manifold cloak with a curved circular insulator. For all the numerical examples, the temperature fields are normalized in this way: $T_i^n = (T_i - T_l)/(T_h - T_l)$, where $T_i = T, T_0$ or T_{ref} for a better visualization effect to display the temperature field comparisons.

3.1. A 2D thermal cloak with circular insulator

As shown in Figure 5(c), a temperature field T_{ref} with uniform gradient is generated by filling Ω_D and Ω_{ins} with iron. When the insulator is presented in Ω_{ins} shown in Figure 5(b), the reference temperature field in Ω_{out} is obviously disturbed with nonparallel temperature contour lines as shown Figure 5(d). To alleviate this temperature perturbation and achieve the thermal cloaking function, the iron and copper are optimally distributed in the design domain Ω_D using the level-set-based topology optimization algorithm.

The optimization result is shown in Figure 6. The normalized temperature field T_n and the discrepancy with the normalized reference temperature field T_{ref}^n are displayed in Figure 7. The temperature contour lines in Ω_{out} region are almost parallel as they are when there is no insulator presented. The temperature difference in Ω_{out} is close to zero and negligible.

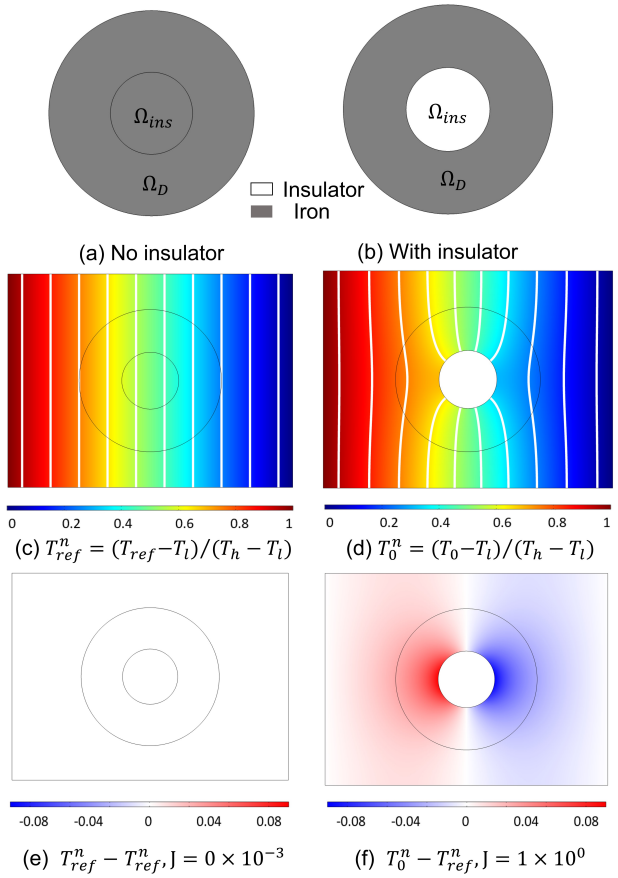

Figure 5: Example 3.1 (a) No insulator in Ω_{ins}, (b) With insulator in Ω_{ins}, (c) Normalized reference temperature field T^n_{ref}, (d)Normalized temperature field T^n_0, (e) T^n_{ref} - T^n_{ref}, (f) T^n_0 - T^n_{ref}

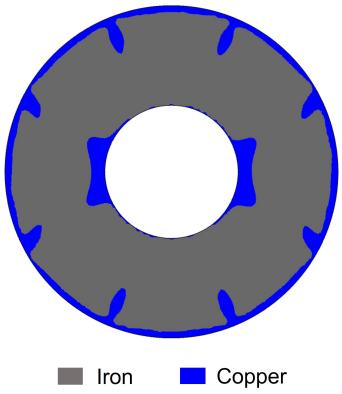

Figure 6: Optimized structure for the thermal cloak with circular insulator

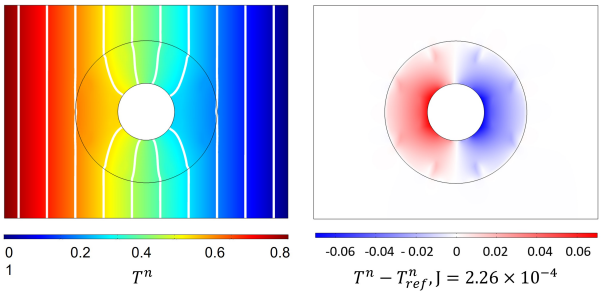

Figure 7: (Example 3.1) Left: the normalized temperature field $T^n = (T - T_l)/(T_h - T_l)$. Right: the normalized temperature difference $T^n - T^n_{ref}$

The objective function $J = 2.26 \times 10^{-4}$, which is small enough to indicate that the insulator is effectively cloaked from being detected by evaluating the temperature field perturbation in Ω_{out}.

The convergence history plot for the thermal cloak with a circular insulator is given in Figure 8. The objective function J is monotonically decreasing as the iteration number goes up. There is no volume constraint imposed on either the iron or the copper in this optimization. The copper accounts for 15.81% of the whole design domain area in Ω_D for the final optimal configuration.

3.2. A 2D thermal cloak with a human-shaped insulator

The second numerical example deals with a similar problem-setting as in shown Figure 1 but with a human-shaped insulator. The optimized structure is exhibited in Figure 9. Again, the temperature field in Ω_{out} with uniform gradient is reproduced as shown in Figure 10 (left). The temperature discrepancy between T^n with the normalized reference temperature field T^n_{ref} in Ω_{ins} is small enough to be neglected. The objective function $J = 7.71 \times 10^{-4}$.

The convergence history plot for the thermal cloak with a human-shaped insulator is shown in Figure 11. In the final optimized configuration, 21.48% of Ω_D are occupied by copper. A clear boundary between the iron and copper is maintained during the optimization process. As a result, little post processing is needed to convert this structure into 3D printable models as shown in Figure 12.

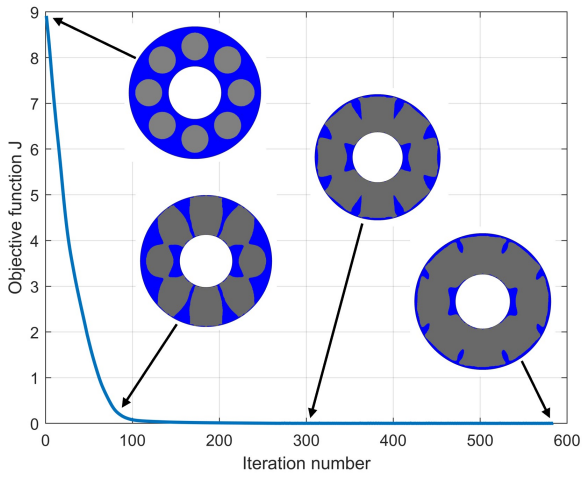

Figure 8: Convergence history for the thermal cloak with circular insulator

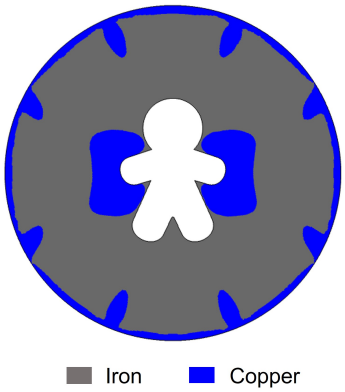

Figure 9: Optimized structure for the thermal cloak with human-shaped insulator

3.3. A 3D thermal cloak with a spherical insulator

In this subsection, we extend the proposed topology optimization scheme to design a 3D solid thermal cloak with a spherical insulator. Few research works have been conducted to design 3D thermal cloaks from the standpoint of numerical optimization. Most of the numerical optimization endeavors focus on only the 2D cases.

As can be seen from Figure 13, the whole computational domain Ω is a cuboid, consisting of the spherical insulator domain Ω_{ins}, the design domain Ω_D with a spherical shell shape and the outer domain Ω_{out}. Two Dirichlet boundary conditions are applied with $T_h =$

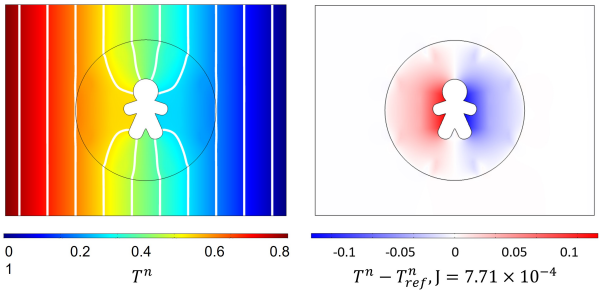

Figure 10: (Example 3.2) Left: the normalized temperature field $T^n = (T - T_l)/(T_h - T_l)$. Right: the normalized temperature difference $T^n - T^n_{ref}$

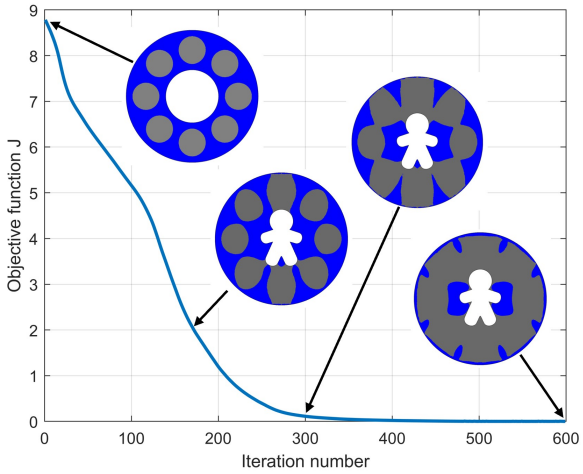

Figure 11: Convergence history for the thermal cloak with human-shaped insulator

$10K$ and $T_l = 0K$ on the left and right side walls, respectively. All other boundaries are adiabatic. Ω_{ins} is the region of interest that we want to cloak. The optimal distribution of iron and aluminum inside the spherical shell Ω_D is sought after using the level-set-based topology optimization algorithm. The outer domain Ω_{out} is always fixed with iron.

As displayed in Figure 14(c), the reference temperature field T_{ref} with uniform gradient is generated by filling the entire computational domain Ω with iron. The temperature field in the outer domain Ω_{out} is clearly disturbed by the introduction of the spherical insulator as shown in Figure 14(d). This disturbance can be identified by the non-parallel temperature contours in Figure 14(d).

The optimal structure for iron in the spher-

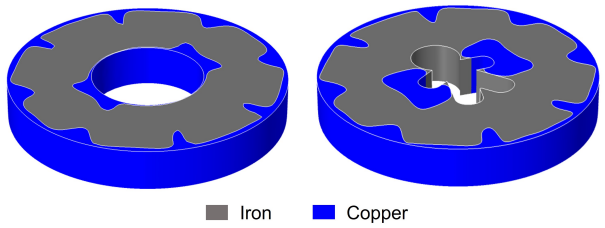

Figure 12: 3D CAD models for the optimized 2D cloaks with left: circular insulator, right: human-shaped insulator

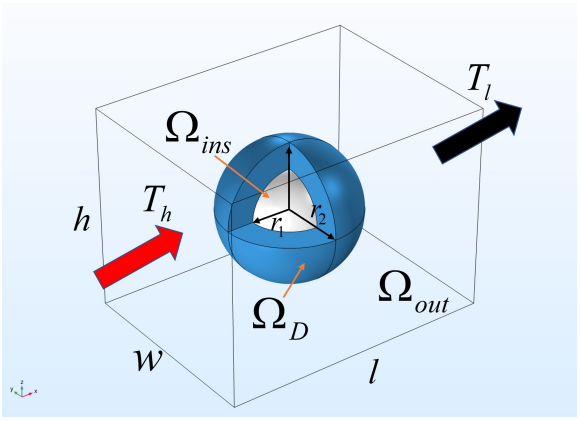

Figure 13: The diagram for a 3D spherical thermal cloak. $w = 3, h = 3, l = 4, r_1 = 0.6, r_2 = 1$. $T_h = 10K, T_l = 0K$. The thermal conductivities for aluminum and iron are set to be $k_{aluminum} = 204W/(m \cdot K), k_{iron} = 67W/(m \cdot K)$.

ical shell design domain Ω_D is given in Figure 15. Both the isometric and orthographic views are provided for the optimized iron configuration. The complementary region of the iron structure in the spherical shell design domain Ω_D will be occupied by aluminum with a higher thermal conductivity. Two cross-sections 1 and 2 are selected in Figure 16(a) to better visualize the optimized structures. The optimal material distribution of iron and aluminum on cross-section 1 and 2 are presented in Figure 16(b) and 16(c), respectively.

As we can see from Figure 17(left), the temperature field with uniform gradient is duplicated in the outer domain Ω_{out} with parallel temperature contours by the optimal distribution of iron and aluminum in the design domain Ω_D. The discrepancy between the normalized temperature field T^n and the normal-

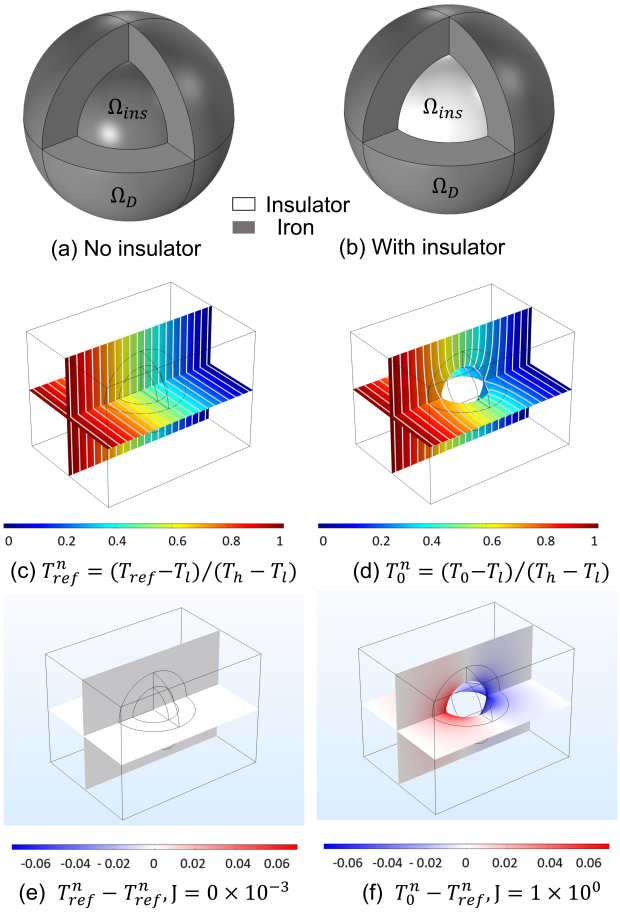

Figure 14: Example 3.3 (a) No insulator in Ω_{ins}, (b) With insulator in Ω_{ins}, (c) Normalized reference temperature field T^n_{ref}, (d)Normalized temperature field T^n_0, (e) T^n_{ref} - T^n_{ref}, (f) T^n_0 - T^n_{ref}

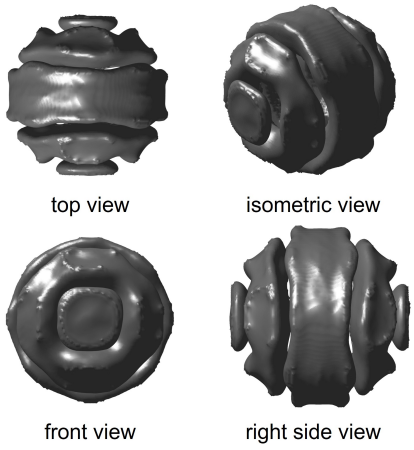

Figure 15: The optimal structure of iron in the design domain Ω_D

ized reference temperature field T^n_{ref} is shown in Figure 17(right). The discrepancy is close

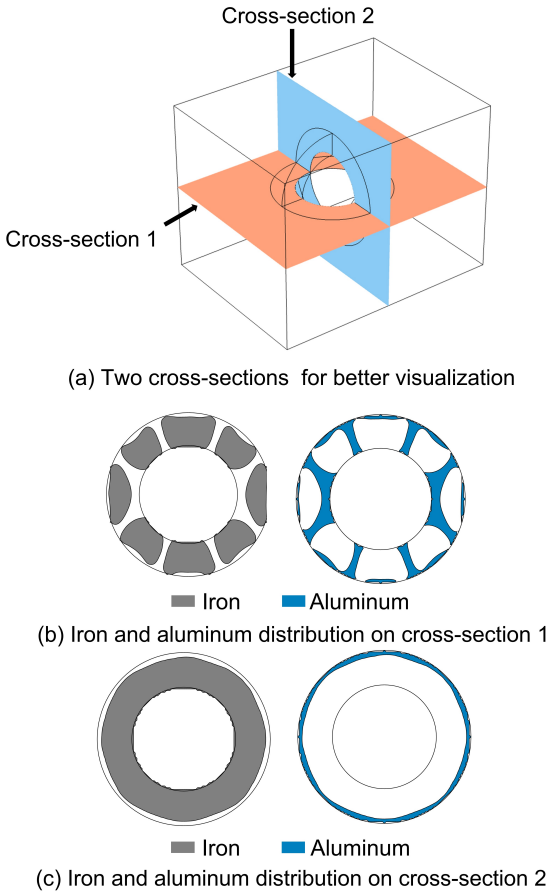

Figure 16: Two cross-sections views for the optimized 3D iron structure

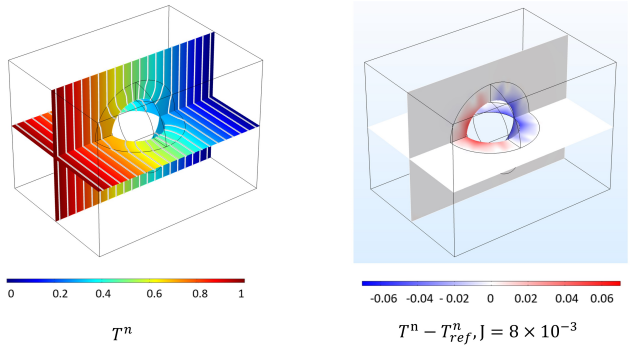

Figure 17: (Example 3.3) Left: the normalized temperature field $T^n = (T - T_l)/(T_h - T_l)$. Right: the normalized temperature difference $T^n - T^n_{ref}$

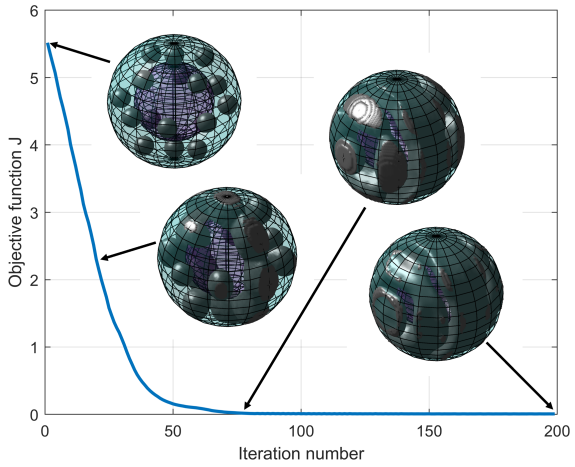

Figure 18: Convergence history for the 3D spherical thermal cloak with iron structure evolution

to zero in the outer domain Ω_{out}, which means the spherical insulator will not be thermally detected by measuring the temperature disturbance in Ω_{out}, thus achieving the cloaking functionality. The objective function $J = 8 \times 10^{-3}$. The convergence history with the iron structure evolution is depicted in Figure 18.

3.4. A manifold thermal cloak with a curved circular insulator

This subsection is devoted to designing a conformal thermal cloak on a general free-form surface using the extended level set method (X-LSM) [42], which has not been investigated in the literature. Most of the existing metadevices for heat flux manipulation purpose are based on 2D planar or solid 3D models. In practical applications, it it not uncommon that the device components that need to be thermally cloaked, e.g., sensors, take an arbitrary free-form shape. To this end, a conformal thermal cloak is strongly desired to provide the necessary cloaking performance.

The problem-setting for a 3D thermal cloak on a spherical surface patch is shown in Figure 19. This manifold model can be obtained by partitioning a semi-spherical surface with two parallel planes. The overall size is $50 \times 70 \times 100$ mm. The shell model thickness is uniform and set to be 1 mm. As can be seen in Figure 19, the whole computational domain Ω consists of a circular insulator domain Ω_{ins}, the ring-shaped design domain Ω_D and the outer domain Ω_{out}. Ω_{ins} is the region of interest that we want to cloak. Two Dirichlet boundary conditions with $T_h = 323K$ and $T_l = 298K$

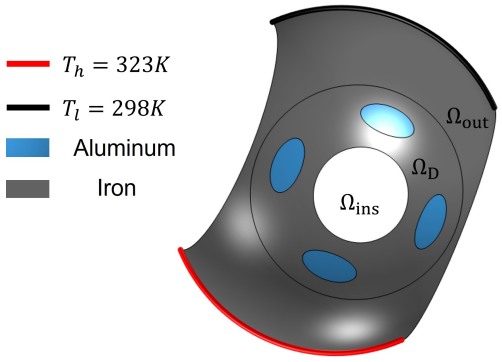

Figure 19: The diagram of a 3D thermal cloak on a spherical surface patch with a circular insulator. The thermal conductivities for aluminum and iron are set to be $k_{aluminum} = 204W/(m\cdot K), k_{iron} = 67W/(m\cdot K)$

are assigned to the boundary edges in red and black, respectively. All other boundaries are set to be adiabatic. The outer domain Ω_{out} is fixed with iron and serve as the evaluation domain to detect the temperature disturbance.

As shown in Figure 20, a temperature field T_{ref} with uniform gradient magnitude is generated by filling Ω_D and Ω_{ins} with iron. When the insulator is presented in Ω_{ins} shown in Figure 20(b), the reference temperature field in Ωout is obviously disturbed with nonparallel temperature contour lines. The initial and optimal designs on the 2D parameter domain and manifold in 3D space are given in Figure 21 and Figure 22, respectively. As can be seen from Figure 23(left), the temperature field in Ω_{out} has been restored. The discrepancy between the normalized temperature field and the normalized reference temperature field is negligible in Ω_{out} shown in Figure 23(right). The final objective function $J = 1.09 \times 10^{-3}$, which is small enough to be considered as a successful thermal cloak. To the best of the author's knowledge, this is the first thermal cloak design on a manifold.

4. Discussions and conclusions

In this study, a level-set-based shape and topology optimization is proposed to design thermal cloaks by distributing two naturally

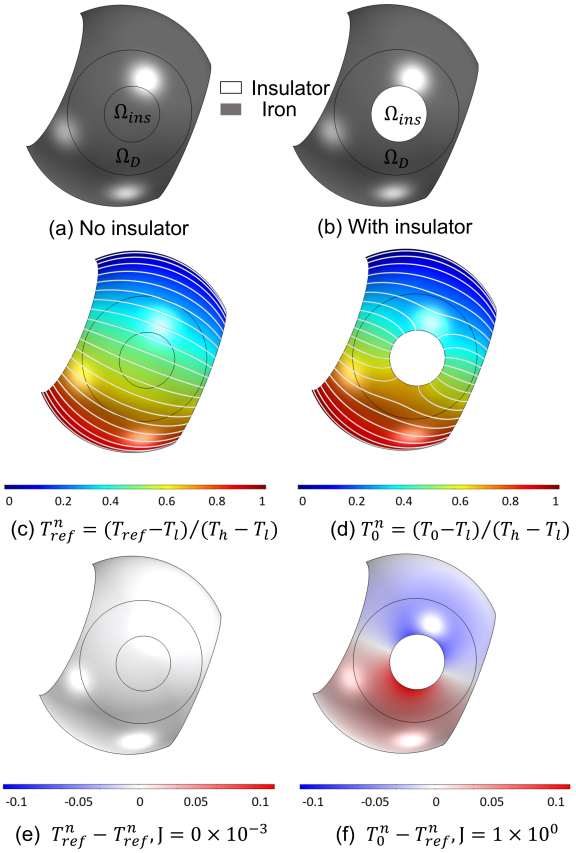

Figure 20: Example 3.4 (a) No insulator in Ω_{ins}, (b) With insulator in Ω_{ins}, (c) Normalized reference temperature field T^n_{ref}, (d)Normalized temperature field T^n_0, (e) T^n_{ref} - T^n_{ref}, (f) T^n_0 - T^n_{ref}

occurring bulk thermal conductive materials to eliminate the temperature disturbance on the evaluation domain caused by the insulator (cloaking region). The optimized structures exhibit the expected cloaking functionality, despite having simple shape and topology. Compared with the transformation thermotics or scattering cancellation methods, the proposed optimization algorithm is advantageous in that the resulting configuration does not possess any anisotropy and non-homogeneity, which could greatly facilitate the physical realization to further validate the cloaking performance.

Four numerical examples are considered in this paper. The first 2D example with a circular cloaking region serves as the benchmark example to draw some comparisons with literature results. It is worth mentioning that

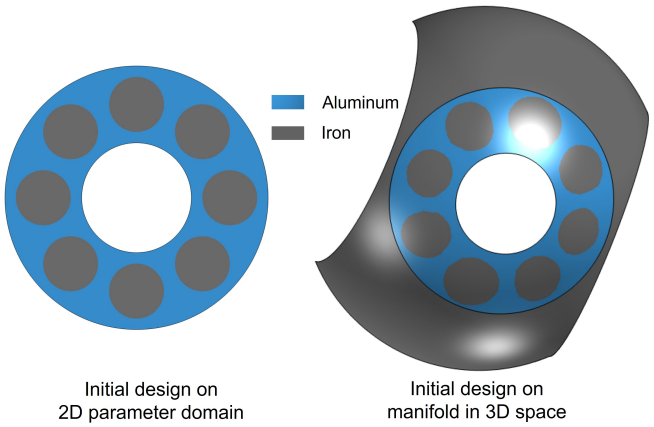

Figure 21: The initial designs for the thermal cloak on a spherical surface patch with a curved circular insulator

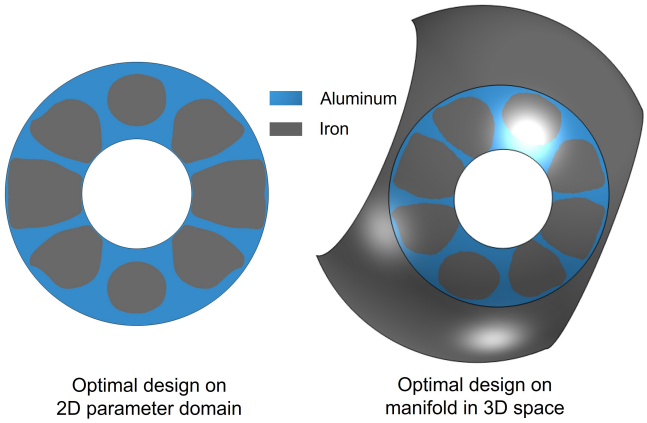

Figure 22: The optimal designs for the thermal cloak on a spherical surface patch with a curved circular insulator

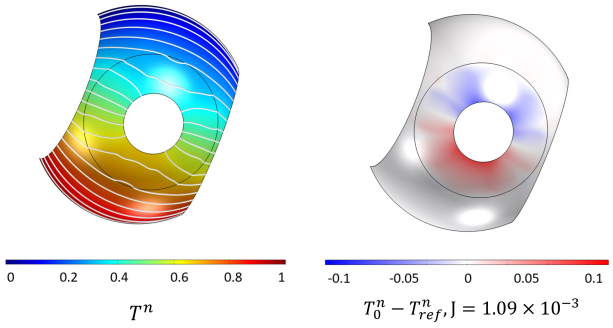

Figure 23: (Example 3.4) Left: the normalized temperature field $T^n = (T - T_l)/(T_h - T_l)$. Right: the normalized temperature difference $T^n - T^n_{ref}$

the optimized structure with a circular insulator has not been seen in the literature, yet it still renders a good cloaking performance. The second 2D example deals with a thermal cloak with a human-shaped insulator. To the best of my knowledge, not many research works have investigated the cloaking of an arbitrary shape. Most of the models considered are canonical shapes, e.g., circular and spherical. The second designed cloak with a human-shaped insulator will trigger more interest in the thermal cloak design for a broader application. The proposed method is then extended to devise a 3D thermal cloak with a spherical insulator. As far as the author is concerned, this is among the first to come up with a 3D thermal cloak design using the numerical optimization method. The last example is concerned with a conformal thermal cloak on a manifold surface optimized using the extended level set method (X-LSM). The thermal cloak on a free-form surface has not been reported in the literature, which could inspire a broader exploration of heat flux manipulation devices on manifolds.

In this paper, we employed the level set framework with only shape derivative, which can only be used to evolve already existing boundaries through, e.g., merging or splitting holes. However, it does not have the hole nucleation capability, i.e., a hole will not be generated inside a local solid region. Thus, the final optimized structure will show some dependence on the initial design. A common strategy to mitigate this dependence is to come up with an initial guess with a decent number of holes, providing enough structural boundaries for subsequent evolution. From this standpoint, the initial shapes selected in Figure 8, 11, 18 and 21 are quite reasonable in providing sufficient boundaries. But we can not claim that they are the best since it is always possible to add more initial holes. Even though they might not be the best initial design, the objective functions J are sufficiently small to be considered as a successful thermal cloak. To be more specific, the objective functions J are 2.26×10^{-4}, 7.71×10^{-4}, 8×10^{-3} and

1.09×10^{-3} for the 2D circular thermal cloak, 2D human-shaped thermal cloak, 3D spherical thermal cloak and conformal manifold thermal cloak, respectively. Another approach is to incorporate topological derivative [56] into the problem formulation, which will enable the hole nucleation to eliminate the dependence on the initial designs.

In the future work, the following aspects worth a further investigation. Firstly, the optimized designs should be numerically verified and experimentally validated to make them more convincing. Secondly, more interesting heat flux manipulation devices should be explored, e.g., thermal camouflage involving thermal radiation.

Acknowledgment

The authors gratefully acknowledge financial support from the National Science Foundation (CMMI-1762287, PFI-2213852), the Ford University Research Program (URP) (Award No. 2017-9198R), and the State University of New York (SUNY) at Stony Brook.

References

[1] H. Chen, C. T. Chan, P. Sheng, Transformation optics and metamaterials, Nature materials 9 (5) (2010) 387–396.

[2] J. B. Pendry, D. Schurig, D. R. Smith, Controlling electromagnetic fields, science 312 (5781) (2006) 1780–1782.

[3] U. Leonhardt, Optical conformal mapping, science 312 (5781) (2006) 1777–1780.

[4] T. Han, X. Bai, D. Gao, J. T. Thong, B. Li, C.-W. Qiu, Experimental demonstration of a bilayer thermal cloak, Physical review letters 112 (5) (2014) 054302.

[5] H. Xu, X. Shi, F. Gao, H. Sun, B. Zhang, Ultrathin three-dimensional thermal cloak, Physical Review Letters 112 (5) (2014) 054301.

[6] C. Fan, Y. Gao, J. Huang, Shaped graded materials with an apparent negative thermal conductivity, Applied Physics Letters 92 (25) (2008) 251907.

[7] H. Chen, C. T. Chan, Acoustic cloaking in three dimensions using acoustic metamaterials, Applied physics letters 91 (18) (2007) 183518.

[8] S. Narayana, Y. Sato, Dc magnetic cloak, Advanced Materials 24 (1) (2012) 71–74.

[9] J.-P. Huang, Theoretical thermotics: transformation thermotics and extended theories for thermal metamaterials, Springer, Singapore, 2020.

[10] L.-J. Xu, J.-P. Huang, Transformation Thermotics and Extended Theories: Inside and Outside Metamaterials, Springer, Singapore, 2022.

[11] S. R. Sklan, B. Li, Thermal metamaterials: functions and prospects, National Science Review 5 (2) (2018) 138–141.

[12] J. Wang, G. Dai, J. Huang, Thermal metamaterial: fundamental, application, and outlook, Iscience 23 (10) (2020) 101637.

[13] S. Yang, J. Wang, G. Dai, F. Yang, J. Huang, Controlling macroscopic heat transfer with thermal metamaterials: Theory, experiment and application, Physics Reports 908 (2021) 1–65.

[14] G. Fujii, Y. Akimoto, M. Takahashi, Exploring optimal topology of thermal cloaks by cma-es, Applied Physics Letters 112 (6) (2018) 061108.

[15] G. Fujii, Y. Akimoto, Cloaking a concentrator in thermal conduction via topology optimization, International Journal of Heat and Mass Transfer 159 (2020) 120082.

[16] X. Shen, Y. Li, C. Jiang, Y. Ni, J. Huang, Thermal cloak-concentrator, Applied Physics Letters 109 (3) (2016) 031907.

[17] W. Sha, M. Xiao, J. Zhang, X. Ren, Z. Zhu, Y. Zhang, G. Xu, H. Li, X. Liu, X. Chen, et al., Robustly printable freeform thermal metamaterials, Nature communications 12 (1) (2021) 1–8.

[18] L. Zhou, S. Huang, M. Wang, R. Hu, X. Luo, While rotating while cloaking, Physics Letters A 383 (8) (2019) 759–763.

[19] S. Narayana, Y. Sato, Heat flux manipulation with engineered thermal materials, Physical review letters 108 (21) (2012) 214303.

[20] R. Hu, W. Xi, Y. Liu, K. Tang, J. Song, X. Luo, J. Wu, C.-W. Qiu, Thermal camouflaging metamaterials, Materials Today 45 (2021) 120–141.

[21] T. Han, X. Bai, J. T. Thong, B. Li, C.-W. Qiu, Full control and manipulation of heat signatures: cloaking, camouflage and thermal metamaterials, Advanced Materials 26 (11) (2014) 1731–1734.

[22] A. Alù, N. Engheta, Achieving transparency with plasmonic and metamaterial coatings, Physical Review E 72 (1) (2005) 016623.

[23] A. Alu, N. Engheta, Plasmonic materials in transparency and cloaking problems: mechanism, robustness, and physical insights, Optics Express 15 (6) (2007) 3318–3332.

[24] M. Imran, L. Zhang, A. K. Gain, Advanced thermal metamaterial design for temperature control at the cloaked region, Scientific Reports 10 (1) (2020) 1–11.

[25] E. M. Dede, T. Nomura, P. Schmalenberg, J. Seung Lee, Heat flux cloaking, focusing, and reversal in ultra-thin composites considering conduction-convection effects, Applied Physics Letters 103 (6) (2013) 063501.

[26] K. P. Vemuri, F. Canbazoglu, P. R. Bandaru, Guiding conductive heat flux through thermal metamaterials, Applied Physics Letters 105 (19) (2014) 193904.

[27] M. Moccia, G. Castaldi, S. Savo, Y. Sato, V. Galdi, Independent manipulation of heat and electrical current via bifunctional metamaterials, Physical Review X 4 (2) (2014) 021025.

[28] Y. Li, X. Shen, Z. Wu, J. Huang, Y. Chen, Y. Ni, J. Huang, Temperature-dependent transformation thermotics: from switchable thermal cloaks to macroscopic thermal diodes, Physical review letters 115 (19) (2015) 195503.

[29] R. Schittny, M. Kadic, S. Guenneau, M. Wegener, Experiments on transformation thermodynamics: molding the flow of heat, Physical review letters 110 (19) (2013) 195901.

[30] K. Hirasawa, I. Nakami, T. Ooinoue, T. Asaoka, G. Fujii, Experimental demonstration of thermal cloaking metastructures designed by topology optimization, International Journal of Heat and Mass Transfer 194 (2022) 123093.

[31] E. M. Dede, T. Nomura, J. Lee, Thermal-composite design optimization for heat flux shielding, focusing, and reversal, Structural and Multidisciplinary Optimization 49 (1) (2014) 59–68.

[32] I. Peralta, V. D. Fachinotti, Á. A. Ciarbonetti, Optimization-based design of a heat flux concentrator, Scientific reports 7 (1) (2017) 1–8.

[33] I. Peralta, V. D. Fachinotti, Optimization-based design of heat flux manipulation devices with emphasis on fabricability, Scientific reports 7 (1) (2017) 1–8.

[34] J. C. Álvarez Hostos, V. D. Fachinotti, I. Peralta, B. A. Tourn, Computational design of metadevices for heat flux manipulation considering the transient regime, Numerical Heat Transfer, Part A: Applications 76 (8) (2019) 648–663.

[35] V. D. Fachinotti, Á. A. Ciarbonetti, I. Peralta, I. Rintoul, Optimization-based design of easy-to-make devices for heat flux manipulation, International Journal of Thermal Sciences 128 (2018) 38–48.

[36] V. D. Fachinotti, I. Peralta, A. E. Albanesi, Optimization-based design of an elastostatic cloaking device, Scientific Reports 8 (1) (2018) 1–8.

[37] J. C. A. Hostos, V. D. Fachinotti, I. Peralta, Computational design of thermo-mechanical metadevices using topology optimization, Applied Mathematical Modelling 90 (2021) 758–776.

[38] M. Seo, H. Park, S. Min, Heat flux manipulation by using a single-variable formulated multi-scale topology optimization method, International Communications in Heat and Mass Transfer 118 (2020) 104873.

[39] W. Sha, Y. Zhao, L. Gao, M. Xiao, R. Hu, Illusion thermotics with topology optimization, Journal of Applied Physics 128 (4) (2020) 045106.

[40] B. Bourdin, Filters in topology optimization, International journal for numerical methods in engineering 50 (9) (2001) 2143–2158.

[41] G. Fujii, Y. Akimoto, Optimizing the structural topology of bifunctional invisible cloak manipulating heat flux and direct current, Applied physics letters 115 (17) (2019) 174101.

[42] Q. Ye, Y. Guo, S. Chen, N. Lei, X. D. Gu, Topology optimization of conformal structures on manifolds using extended

level set methods (x-lsm) and conformal geometry theory, Computer Methods in Applied Mechanics and Engineering 344 (2019) 164–185.

[43] X. D. Gu, S.-T. Yau, Computational conformal geometry, Vol. 1, International Press Somerville, MA, 2008.

[44] J. A. Sethian, A. Wiegmann, Structural boundary design via level set and immersed interface methods, Journal of computational physics 163 (2) (2000) 489–528.

[45] G. Allaire, F. Jouve, A.-M. Toader, Structural optimization using sensitivity analysis and a level-set method, Journal of computational physics 194 (1) (2004) 363–393.

[46] M. Y. Wang, X. Wang, D. Guo, A level set method for structural topology optimization, Computer methods in applied mechanics and engineering 192 (1-2) (2003) 227–246.

[47] S. Osher, R. Fedkiw, K. Piechor, Level set methods and dynamic implicit surfaces, Appl. Mech. Rev. 57 (3) (2004) B15–B15.

[48] K. K. Choi, N.-H. Kim, Structural sensitivity analysis and optimization 1: linear systems, Springer Science & Business Media, 2004.

[49] G. Allaire, A review of adjoint methods for sensitivity analysis, uncertainty quantification and optimization in numerical codes, Ingénieurs de l'Automobile 836 (2015) 33–36.

[50] R. S. Hamilton, The ricci flow on surfaces, in: Mathematics and general relativity, Proceedings of the AMS-IMS-SIAM Joint Summer Research Conference in the Mathematical Sciences on Mathematics in General Relativity, Univ. of California, Santa Cruz, California, 1986, Amer. Math. Soc., 1988, pp. 237–262.

[51] W. Zeng, X. D. Gu, Ricci flow for shape analysis and surface registration: theories, algorithms and applications, Springer Science & Business Media, 2013.

[52] J. Tian, M. Li, Z. Han, Y. Chen, X. D. Gu, Q. Ge, S. Chen, Conformal topology optimization of multi-material ferromagnetic soft active structures using an extended level set method, Computer Methods in Applied Mechanics and Engineering 389 (2022) 114394.

[53] J. Tian, X. Zhao, X. D. Gu, S. Chen, Designing ferromagnetic soft robots (ferrosoro) with level-set-based multiphysics topology optimization, in: 2020 IEEE International Conference on Robotics and Automation (ICRA), IEEE, 2020, pp. 10067–10074.

[54] X. Xu, S. Chen, X. D. Gu, M. Y. Wang, Conformal topology optimization of heat conduction problems on manifolds using an extended level set method (x-lsm), in: International Design Engineering Technical Conferences and Computers and Information in Engineering Conference, Vol. 85390, American Society of Mechanical Engineers, 2021, p. V03BT03A030.

[55] X. Xu, X. D. Gu, S. Chen, Shape and topology optimization of conformal thermal control structures on free-form surfaces: A dimension reduction level set method (dr-lsm), Computer Methods in Applied Mechanics and Engineering 398 (2022) 115183.

[56] M. Burger, B. Hackl, W. Ring, Incorporating topological derivatives into level set methods, Journal of computational physics 194 (1) (2004) 344–362.